Control Oriented Modeling and Optimization of One Dimensional Packed Bed Model of Underground Coal Gasification

Ali Arshad Uppal[a], Aamer Iqbal Bhatti[b], Erum Aamer[b], Raza Samar[b], Shahid Ahmed Khan[a]

[a] *COMSATS Institute of Information Technology, Islamabad, Pakistan*
[b] *Mohammad Ali Jinnah University, Islamabad, Pakistan*

Abstract

To account for nonlinear nature and huge model uncertainties of underground coal gasification (UCG) process, a robust model based control strategy is to be employed. The available models in the literature do not lend themselves to control applications easily. In this work a control oriented one dimensional (1-D) packed bed model of UCG is developed, which can be used in a closed loop configuration with a robust controller to maintain a desired heating value of the exit gas mixture by manipulating the flow rate of injected gases. The model is also capable of predicting time and space profiles of some important parameters, which include solid temperature, composition of exit gas mixture, rates of different chemical reactions and expected life of the UCG reactor in response to different operating conditions and coal properties. Most of these parameters are either impossible or very expensive to measure. There is uncertainty in some coal properties which is addressed by optimizing few input parameters using sequential quadratic programming (SQP) algorithm, a nonlinear optimization technique. The model results are compared with actual field trials which show a good agreement for the calorific value of exit gas.

Keywords:
Underground coal gasification (UCG), 1-D packed bed model, sequential quadratic programming (SQP) and optimization.

1. Introduction

Fossil fuels (coal, natural gas and oil) cover 84% of World's energy demand, of which the share of coal is 28% [1]. The advantages of coal over other fossil fuels are its relative abundance, and its low and stable cost [2]. Thar coal field, situated in southern part of Pakistan contains 175 billion tons of lignite coal [3]. By considering type of coal, depth and thickness of coal seam and location of water aquifers under the surface of earth, UCG project Thar has launched a project of UCG in Block-V of Thar coalfield to address the energy crisis of the country.

Fig. 1 illustrates the process of UCG in a simplified manner. Before the start of process, two wells (inlet and outlet) are drilled from surface to the coal seam, and a link is established between the drilled wells to allow the flow of gas through coal bed. After link establishment coal seam is ignited and a mixture of gas is injected in to the inlet well. The inlet gas consists of air/O_2 or air and H_2O. The gasifier is divided in to three zones: oxidation zone, reducing zone and drying and pyrolysis zone. In oxidation zone, char oxidation reaction takes place which increases the temperature of the UCG reactor. In reduction zone, the important gasification reactions take place which generate the desired syngas (a mixture of CO and H_2). In drying and pyrolysis zone, the coal seam is initially dried and then pyrolysed. The estimated temperature ranges for different zones is also depicted in Fig. 1. The product gases including syngas, come out from the outlet well. The syngas can be used as a fuel for combined cycle turbines (CCT) for electricity generation using Integrated Gasification Combined Cycle (IGCC) power plants [5] or as a chemical feedstock [2], and [6].

Four different types of mathematical models of UCG are found in the literature: channel model, packed bed model, coal block model and process model [2]. In channel model, injection and production wells are physically linked by a horizontal borehole. The coal is gasified at the perimeter of the channel [7]. This type of method is used for the high rank coal, which has very poor permeability e.g. anthracite. Magnani et al., [7] and [8] developed two channel models of UCG, which represent the system dynamics in one and two space dimensions respectively. In packed bed modeling technique a link is established between inlet and outlet wells either by reverse combustion linking (RCL)

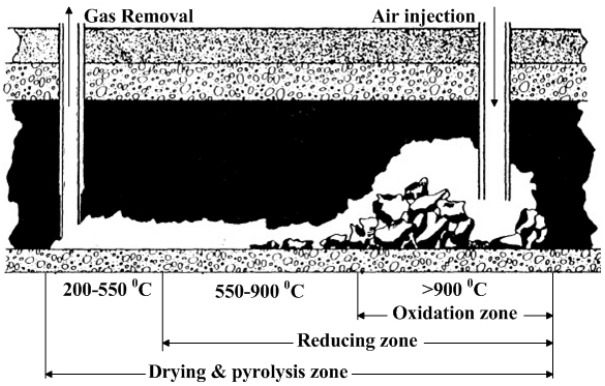

Figure 1: Schematic of UCG process [4]

or by fracturing the coal seam using pressurized air or chemical explosives [9]. The resultant high permeability zone is ignited and then gasified by suitable inlet gases [10]. This technique is used for low and medium rank coals, e.g. lignite and sub-bituminous, which have relatively higher permeability than anthracite. Winslow et al., [11], Thorsness et al., [12], Khadse et al., [6] and Perkins et al., [13] considered UCG process as a packed bed reactor. The coal block modeling technique considers coal seam as a wet slab of coal, which is initially dried and then gasified. Perkins et al., [14] has considered coal block model for UCG process. Process models calculate the cavity growth of the UCG reactor with time in a three dimensional (3-D) space, Beizen et al., [15] considered this type of modeling. Solution of all the models evolve in both time and at least one space dimension except for channel models. In channel models the solution is function of space only. These models are only used for quantitative description of UCG process, none of these models are used for UCG process control.

The control of UCG is an emerging area of research and is so for limited to the laboratory scale UCG setups. In literature only the model free control of lab scale UCG rig is found [16] and [17], and there is no evidence of model based control of UCG process. In our earlier work [18] a simplified time domain model of UCG is developed and then a robust model based sliding mode control [19] strategy is successfully implemented on the developed model. The simplified model ignores some important aspects of the UCG process and therefore falls short of predicting the actual UCG phenomena. In the current work limitations of the simplified model have been addressed and the results of the current model have a better resemblance with the actual field trials.

The primary objective of this research work is to develop a control oriented mathematical model for UCG process, which can assist the actual field trials and in the subsequent control of the process. In this work an already existing model of [20] is adapted with some modifications in model structure and solution strategy. The model is capable of predicting the chemical composition of the product gas as a function of the injected gas composition and rate as well as how it might vary with coal properties. The input stoichiometric coefficients for coal pyrolysis reaction are also optimized in order to compensate for the uncertainty in some coal properties. The optimization is performed by using a constrained nonlinear optimization technique, based on SQP algorithm. The heating value of the model is compared with field trials in order to validate the model. The model can also be used in a feed back configuration with a robust controller, which manipulates the flow rate of injected gas mixture to maintain a desired calorific value of exit gas, as discussed in [18]. The employed optimization technique only compensates for uncertainties in coal parameters, which are used to calculate stoichiometric coefficient matrix. There are a lot of other uncertainties and disturbances due to model assumptions and in-situ conditions respectively, which can be mitigated by using robust control algorithms.

The rest of the article is arranged as: The reactor model of UCG is discussed in Section 2. Section 3 explains the solution strategy for solving the model equations. In Section 4 capabilities of the solved model are discussed. Results of the solved model and field trials are compared in Section 5, and the paper is concluded in Section 6.

2. UCG Reactor Model

This Section discusses 1-D packed bed model of UCG, which is adapted from [20]. The salient features and assumptions considered for syngas model are listed below:

- Model of syngas consists of eight gas species: CO, CO_2, H_2, H_2O, CH_4, N_2, O_2, and tar (a pseudo specie used to close the stoichiometry of coal pyrolysis [20]) and two solid species: coal and char.
- Equations for energy and mass balances (derived from laws of conservation of enrgy and mass respectively) of gas and solid species are written separately for syngas model.
- 1-D assumption is made for mass and energy balances of gas and solid species. This approximation ignores some important multidimensional effects like heat losses and cavity growth of UCG reactor, but it makes the model simple.
- A set of nine chemical reactions is used to describe the chemical kinetics of the process.
- Heat source generated from chemical reactions is written separately for solid and gas phases, which neglects detailed interaction at the point of reaction between the two phases.
- All the conductive transport is lumped in solid phase, neglecting all the accumulation terms in gas phase, this approximation is actually the part of quasi-steady state assumption. According to this assumption convective inter phase and heat source terms for chemical reactions dominate the accumulation terms at all points in the system. This assumption is valid due to low density of gas phase as compared to solid phase, and also due to the large differences in the characteristic time of both phases.
- Coal seam is assumed to be a porous medium, and Darcy's law is used as momentum balance for gas phase.
- The particle size and porosity of coal bed is assumed to be constant.

2.1. Mathematical Equations

2.1.1. Solid Phase Mass Balance

The mass balance equation for solids explains the effect of different chemical reactions on the rate of change of solid density.

$$\frac{\partial}{\partial t}\rho_i = M_i \sum_{j=1}^{9} a_{s_{ij}} R_j \tag{1}$$

where ρ_i is the density of *ith* solid (kg/m^3), a_{sij} is the stoichiometric coefficient of *ith* solid specie in *jth* chemical reaction (a_{sij} is positive for products and negative for reactants), R_j is rate of *jth* chemical reaction (mol/m^3/s), M_i is the molecular weight of solid component *i* (kg/mol) and *t* is variable for time (s).

The chemical reactions and there kinetics are given in Section **??**.

2.1.2. Solid Phase Energy Balance

Eq. (2) shows that how does solid temperature change with time due to heat transfer through conduction (between adjacent coal layers) and convection (inter phase heat transfer caused by the movement of gases), and heat of chemical reactions.

$$\begin{aligned} \frac{\partial T_s}{\partial t} &= \frac{\frac{\partial}{\partial x}\left[(1-\phi)k\frac{\partial T_s}{\partial x}\right] + h_T(T - T_s) - H_s}{C_s} \\ C_s &= \sum_{i=1}^{2} \rho_i c_{s_i} \\ H_s &= \sum_{j=1}^{5} \Delta H_j R_j \end{aligned} \tag{2}$$

where T_s and T are solid and gas phase temperatures respectively (K), ϕ is coal bed porosity, k is the effective thermal conductivity of solids (J/m/s/K), h_T is the heat transfer coefficient (J/m^3/s/K), c_{s_i} is the specific heat capacity of component i (J/m/K) and ΔH_j is the heat of the reaction for heterogeneous (solid-gas) reactions (J/mol) and x is variable for reactor length (m).

The description of h_T and k is given in Eq. (A.1) and Eq. (A.3) respectively.

2.1.3. Gas Phase Mass Balance

The concentration of a gas is changed when it moves from inlet to outlet. The change is brought by the chemical reactions and superficial gas phase velocity. Superficial velocity in porous media, is a hypothetical velocity of gas phase considered over whole cross sectional area by ignoring the solid phase [21].

$$\frac{dC_i}{dx} = \frac{1}{u_g}\left(-C_i\frac{du_g}{dx} + \sum_{j=1}^{9} a_{ij}R_j\right) \tag{3}$$

where C_i the concentration of *ith* gas (mol/m^3), u_g is superficial gas velocity (m/s) and a_{ij} is the stoichiometric coefficient of *ith* gas in *jth* chemical reaction (a_{ij} is positive for product gases and negative for reactant gases).

2.1.4. Gas Phase Energy Balance

The gas temperature is only affected by convective heat transfer effect and heat of chemical reactions, as gas moves in the reactor. The accumulation terms are neglected due to quasi-steady state assumption.

$$\begin{aligned}\frac{dT}{dx} &= -\frac{1}{u_g C_g}\left[h_T(T - T_s) + H_g\right] \\ C_g &= \sum_{i=1}^{8} C_i c_{p_i} \\ H_g &= \sum_{j=6}^{9} \Delta H_j R_j\end{aligned} \tag{4}$$

where c_{p_i} is the molar heat capacity for *ith* gas and H_j is the heat of the reaction for homogeneous (gas-gas) reactions (J/mol).

2.1.5. Momentum Balance Equation

The solid species in the model are immovable, so momentum balance is only written for gas phase using Darcy's law.

$$\frac{dP}{dx} = -\frac{u_g \mu}{2K} \tag{5}$$

where P is the gas pressure (Pa), K is the gas permeability coefficient (m^2), and μ is the viscosity (Pa.s).

2.1.6. Equation Of State

Ideal gas law is used to relate the gas phase pressure, temperature and concentration.

$$\begin{aligned}C_T &= \frac{P}{RT} \\ C_T &= \sum_{i=1}^{8} C_i\end{aligned} \tag{6}$$

where R is universal gas constant (m^3.Pa/mol/K).

2.1.7. Gas Phase Velocity

The equation for the gas phase velocity is derived from Eq. (3) and Eq. (6)

$$\frac{d}{dx}u_g = -\frac{u_g}{P}\frac{dP}{dx} + \frac{u_g}{T}\frac{dT}{dx} + \frac{RT}{P}\sum_{i=1}^{8}\sum_{j=1}^{9} a_{ij}R_j \tag{7}$$

3. Method Of Solution

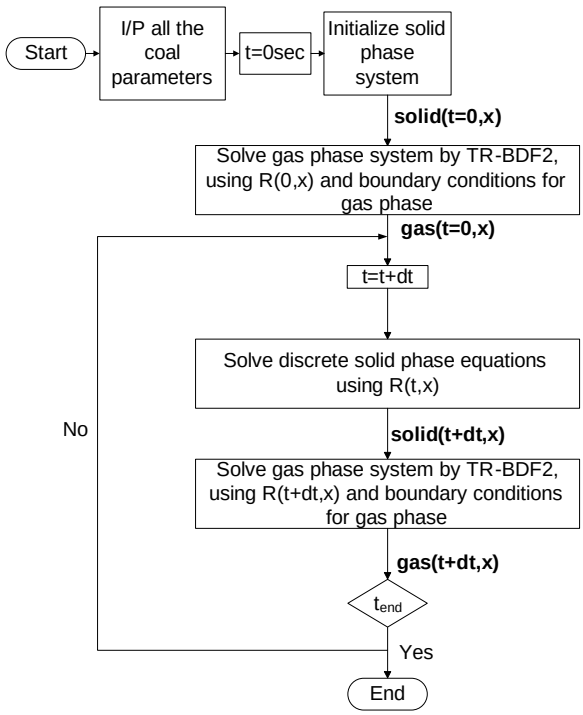

Figure 2: Solution strategy for the UCG reactor model

The model yields two sets of equations, a set of eleven first order gas phase ordinary differential equations (ODE's) in length domain (Eq. (3) for all gases, and Eqs. (4), (5) and (7)) and a set of three solid phase partial differential equations (PDE's) in time and space (Eq. (1) for each solid and Eq. (2)). These two sets of equations can be used for subsequent control of the UCG process. The gas phase equations are solved simultaneously as a boundary value problem, marching from inlet to outlet. Due to the stiff nature of the gas phase ODE's, they are solved using TR-BDF2, an implicit Runge-Kutta algorithm [22]. The gas phase ODE's become stiff due to large increase in solid and gas temperatures (see Fig. 3) at reaction front. Reaction front is a location along the reactor's length where heterogeneous (gas-solid) reactions take place (zoomed area in Fig. 4). The solid phase equations are discretized using forward Euler and explicit finite difference methods [23] for Eq. (1) and Eq. (2) respectively, and then solved for new time. The discrete solid phase equations are given in Appendix B.

The complete solution strategy is given in Fig. 2. The solution starts by initializing coal parameters and solid phase equations and then solving gas phase system for generating its initial conditions. The initialization of solid temperature mimics ignition of coal bed, which is very critical for solution of the system. When solution progresses in time the solid phase system is updated first, and then the gas phase system is advanced in time using the updated solution of solid phase system. Solid phase system uses reaction rates for previous time: R(t,x), where as gas phase system uses the updated reaction rates: R(t+dt,x). The equations for reaction rates given in Appendix A are written within the gas and solid phase systems.

Each solution variable is a 2-D matrix, which shows the behavior of the variable with respect to time and length. The solution evolves in time due to the solid phase system and the change in the length is brought by the gas phase system. Therefore the coupling of the two systems is very critical.

Table 1: Input parameters for UCG packed bed model

Sr	**Parameter**	**Value**
1	Length of reactor	25 m
2	Coal type	Lignite B
3	Flow rate of inlet gas mixture G	2 mol/m^{2}sec (for Sec. 4)
4	Inlet gas composition	air (21% O_2 and 79% N_2) during ignition and gasification
5	Temperature of gas at the inlet ($T_{x=0}$)	430 K
6	Pressure of gas at the inlet ($P_{x=0}$)	618.0825 KPa
7	Velocity of gas phase at the inlet ($u_{g_{x=0}}$)	$\left(\frac{G}{CT_{x=0}}\right)$
8	Initial coal density	1250 kg/m^3

The model is simulated in two modes: ignition and gasification. During ignition, coal bed is heated up to initial 0.1 m for 1000 secs. Due to the absence of steam during ignition phase no gasification reaction takes place, the only reaction taking place in this phase is coal pyrolysis, which converts coal in to char. When gasification phase starts, a sufficient amount of steam is assumed to be present or is allowed to enter the UCG reactor. An optimum amount of steam is required during the gasification process to facilitate the production of syngas. During the field trials the inlet gas does not contain any steam. This means water which intrudes in to the UCG reactor from surrounding aquifers and moisture contained in the coal converts in to steam and assists the gasification reactions. The water intrusion can be controlled by varying the pressure gradient within the reactor [24].

Some of the important parameters used for simulation of the UCG reactor model are listed in Table. 1.

4. Model Capabilities

Some important results of the model are discussed in subsequent paragraphs, which show that the solved model is capable of predicting some important parameters of the UCG process.

Fig. 3 shows the movement of length profiles of solid and gas temperatures with time. For all the given cases, gas temperature follows the solid temperature, the gas temperature increases if it is less than the solid temperature and it decreases if it is greater than solid temperature. The solid temperature profiles contain a lot of information, e.g. for second case (18300 secs) the left boundary of solid temperature profile indicates the location of reaction front and its right boundary is showing pyrolysis front (location along the reactor length where pyrolysis reaction takes place). At the reaction front solid temperature suddenly rises to its peak value due to highly exothermic char oxidation reaction. When solid temperature moves towards pyrolysis front its value decreases due to endothermic steam gasification and CO_2 gasification reactions. The hump in the solid temperature near pyrolysis front is due to exothermic pyrolysis reaction. The region before the reaction front is called rubble zone, the region between reaction front and pyrolysis front is called the reaction zone, and the region beyond pyrolysis front contains unreacted coal.

The reaction zone at 18300 secs is shown in Fig. 4. For avoiding complexity in solution of the system, all the reversible reactions are considered to proceed in the forward direction only. All of the reactions have different activation energies, so they are activated at different temperatures. Due to high activation energy of gasification reactions, the peaks of the reaction rates of steam gasification (R_3) and CO_2 gasification (R_4) reactions occur at the reaction front, where solid temperature has its maximum value. The reaction rates of heterogeneous char-gas reactions: char oxidation (R_2), steam gasification (R_3), CO_2 gasification (R_4) and methanation (R_5) are significant near the reaction front, where char is in excess. The char oxidation reaction rate (R_2) is also very sensitive to the amount of O_2 in the inlet gas mixture. The rate of pyrolysis reaction (R_1) is maximum near the pyrolysis front, where the coal is in excess. The water gas shift reaction rate (R_6) almost spans the whole reaction zone, except the region where concentration of steam and solid temperature have low values. It can be seen from Fig. 4 that the process of UCG is dominated by three reactions: coal pyrolysis, char oxidation and steam gasification.

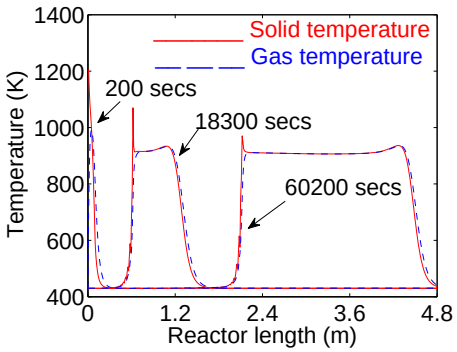

Figure 3: Profiles of solid and gas temperatures along reactor's length at different simulation times.

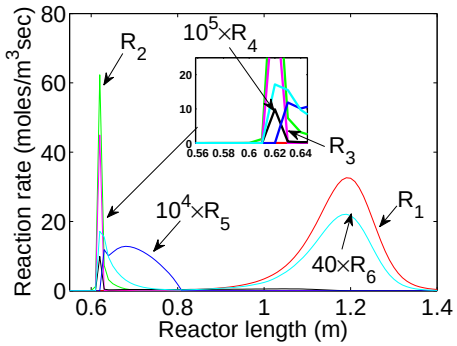

Figure 4: Rates of selected chemical reactions along the length of reactor at 18300 secs.

Fig. 5 shows dry gas mole fractions along length at 18300 secs. O_2 coming from the inlet well remains unreacted until the reaction front, where it is entirely consumed by char oxidation reaction giving rise to CO_2 in the reactor. Mole fraction of CO_2 remains constant until the pyrolysis front, where it slightly decreases due to less increase in the concentration of CO_2 in pyrolysis reaction as compared to the other volatiles. CO is generated at the reaction front by steam gasification reaction, when CO moves towards the outlet well it is completely consumed by water gas shift reaction before its regeneration by pyrolysis reaction at pyrolysis front. Like CO, H_2 is also produced by the steam gasification reaction, on its way towards the exhaust well its concentration is first increased by water gas shift reaction (a small increase) and then by pyrolysis reaction (a large increase). CH_4 and TAR are the products of pyrolysis reaction, which are produced at pyrolysis front. Fig. 5 also shows that concentration of gases and hence mole fractions only change within the reaction zone.

The densities of coal and char are show in Fig. 6. Coal is initially dried and then pyrolysed (heating in the absence of O_2) by heat coming from the reaction zone, the products of pyrolysis are char and gases which reside in the reaction zone to assist other reactions. Char is produced at the pyrolysis front and consumed at the reaction front, between the boundaries of reaction zone it remains constant. Therefore it can be concluded that reactions involving solids occur at the boundaries of reaction zone.

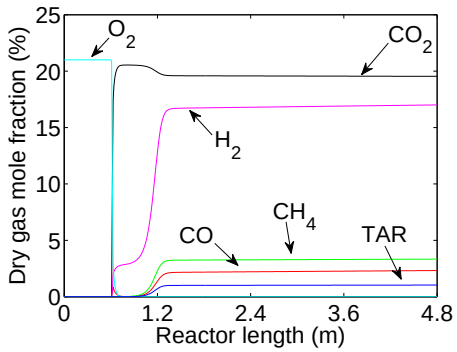

Figure 5: Mole fraction of gases without steam along the length of reactor at 18300 secs.

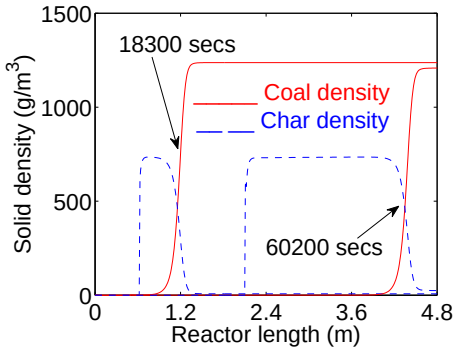

Figure 6: Solid phase densities as a function of length for different simulation times.

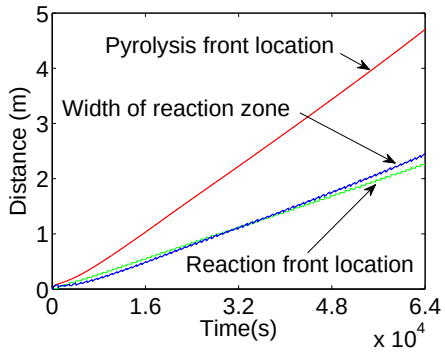

Figure 7: Movement of pyrolysis and reaction fronts with time.

Fig. 7 shows that pyrolysis front and reaction front move from inlet well to outlet well with the passage of time. The results in Fig. 7 give a rough approximation of the expected life of UCG reactor. The instantaneous difference between locations of pyrolysis and reaction fronts gives instantaneous width of the reaction zone. Fig. 7 shows that reaction zone is widening with the passage of time, this information is also implicitly provided by Fig. 3 and Fig. 6. Fig. 7 also gives an idea about the expected life of the UCG reactor. The fuel for the reactor is coal and char. When pyrolysis front reaches the outlet well (25 m) the coal bed is almost exhausted. The process ends when all the char is consumed in the reactor, which is indicated by reaction front approaching the outlet. Actually all the chemical reactions take place between reaction and pyrolysis fronts (see Fig. 4), therefore when reaction front approaches the outlet well all the reactions stop and the process ends.

5. Model Validation

It is important to highlight that the solution of the model and hence model validation is very sensitive to the initial conditions of solid phase equations and boundary conditions for gas phase system. In addition, the discretization in time and length for solid and gas phases respectively should be able to capture the complete reactor dynamics. Therefore it is very important to choose a maximum step size for time and length which can avoid divergence of solution and also provide all the necessary information about the model by avoiding the computational complexity.

5.1. Experimental setup

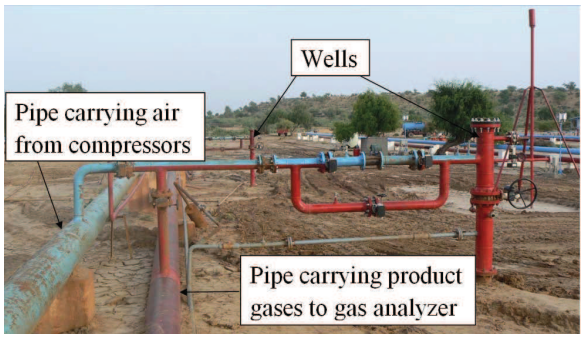

Figure 8: Field area showing setup for UCG.

The site area consists of control and analysis area and a rectangular field. The important components in the control and analysis area are LP (Low Pressure) and HP (High Pressure) compressors, control valve and gas analyzer. LP compressors are used to supply air during gasification, where as HP compressors are used as a source of compressed air during well linking phase. The wells are linked using reverse combustion linkage (RCL) technique [25]. Control valve is placed in a control room and it is used to manipulate flow rate of air coming from the compressors. After separation of steam from the exit gas mixture, the gases are sent to the gas analyzer. The GAS 3100 R coal gas/syngas analyzer [26] measures the mole fraction of gases and then calculates the heating value of the exit gas mixture. The technologies used to measure mole fraction of different gases are listed below.

- CO, CO_2, CH4 and TAR are measured by Dual beam Non-Dispersive Infra-Red (NDIR) detectors.
- H_2 is measured by Thermal conductivity (TCD) detector.
- A galvanic fuel cell is used to determine the % volume content of O_2 in the sample gas.

Molar fraction of N_2 is measured by using the measurements of other gases. The heating value of gases is calculated by using following relationship

$$\begin{aligned} HV_{exp} &= m_{CO_{exp}} H_{CO} + m_{TAR_{exp}} H_{TAR} \\ &+ m_{CH_{4_{exp}}} H_{CH_4} + m_{H_{2_{exp}}} H_{H_2} \end{aligned} \tag{8}$$

where HV_{exp} is the experimental heating value of the exit gas mixture (KJ/m^3), $m_{C_{i_{exp}}}$ is the experimental percentage mole fraction of *ith* gas and H_i is heat of combustion of *ith* gas (KJ/m^3).

The field shown in Fig. 8 spans 18750 m^2 area (150 m long and 125 m wide) and contains an array (7×6) of wells connected by a network of pipes, two consecutive wells are 25 m apart from each other. The blue pipes in Fig. 8 take air at a specific pressure and flow rate to the injection well and the red pipes carry product gas mixture to the gas analyzer from the outlet well/s.

The experiment was performed on a pair of wells. The subjected coal seam was 144 m to 149 m deep and 5 m thick.

5.2. Optimization

Two different sets of data are used for optimization and model validation. There is uncertainty in the ultimate and proximate analysis of coal and char which is compensated by optimizing some parameters. The proximate and ultimate analysis of coal and char have an impact on stoichiometric balance of chemical reactions given in Table. A.2, especially on coal pyrolysis reaction. Moles of H_2 ($a_{3,1}$), CH_4 ($a_{5,1}$) and Char ($a_{s_{2,1}}$) are inputs for balancing the coal pyrolysis reaction, so there values effect the moles of other product gases. Therefore uncertainty in coal analysis is compensated by optimizing $a_{3,1}$, $a_{5,1}$ and $a_{s_{2,1}}$. The constrained nonlinear optimization is performed using sequential quadratic programing (SQP) algorithm [27], which is defined in Eq. (9).

$$min_x f(x), \quad such\ that \begin{cases} h(x) = 0 \\ g(x) \leq 0 \end{cases} \tag{9}$$

where $\mathbf{x} \in \Re^n$ is a vector of optimization variables, $f : \Re^n \rightarrow \Re$ is a scalar objective function, $h : \Re^n \rightarrow \Re^m$ defines the equality constraint, $g : \Re^n \rightarrow \Re^p$ defines the inequality constraint. f is a quadratic function of $\mathbf{x}$ and h and g are affine functions of $\mathbf{x}$.

The inequality constraint g makes sure that moles of CO remain greater than zero in coal pyrolysis reaction. The equality constraint h is not used in the optimization routine.

The definitions of $\mathbf{x}$, f and g are given in Eq. (10).

$$\begin{aligned} x &= \begin{bmatrix} a_{3,1} & a_{5,1} & a_{s_{2,1}} \end{bmatrix}, \quad x_{lb} < x < x_{ub} \\ f &= w \times \left[\frac{\sum_{t=1}^{n} \left(HV_{sim,t} - HV_{exp,t} \right)}{\sum_{t=1}^{n} HV_{exp,t}} \right]^2 \\ g &\leq 0 \\ g &= Ax - b \\ &where, \\ A &= \begin{bmatrix} c_1 & c_2 & c_3 \end{bmatrix} \end{aligned} \tag{10}$$

where $\mathbf{x_{lb}} = \mathbf{x} - \mathbf{0.05x}$ and $\mathbf{x_{ub}} = \mathbf{x} + \mathbf{0.1x}$ are lower and upper bounds on $\mathbf{x}$ respectively, w is a weighting factor which is used to suppress the objective function, $\mathbf{HV_{sim}}$ is simulated heating value of product gas mixture (KJ/m^3) which is a function of multiple variables including $\mathbf{x}$. $\mathbf{A} \in \Re^{1\times3}$ is a vector of constants and b is also a constant.

The value of HV_{sim} can be computed by using Eq. (11)

$$\begin{aligned} HV_{sim} &= m_{CO}H_{CO} + m_{TAR}H_{TAR} \\ &+ m_{CH4}H_{CH_4} + m_{H_2}H_{H_2} \\ m_{C_i} &= 100 \times \frac{C_i}{\tilde{C_T}} \\ \tilde{C_T} &= \sum_{i=1, i\neq4}^{8} C_i \end{aligned} \tag{11}$$

where m_{C_i} is percentage mole fraction of *ith* gas and $\tilde{C_T}$ (mol/m^3) is total concentration of gases without steam.

The above equations show that the parameters are optimized using results of experimental data obtained from the site. During optimization constraints are imposed on each parameter to make sure that these parameters have the same physical limitations as on site. Once the parameters are optimized the results are validated against different set of experimental data at different conditions. However the operating conditions like composition of inlet gas mixture, flow rate and pressure of injected gases and amount of steam in the UCG reactor can be kept same for different experiments.

5.3. Result Comparison

After optimization, results of the solved model are compared with the experimental data from field trials. The experimental data is taken after every one hour, where as the discretized solid phase equations in Appendix B are solved with a step size of 20 secs.

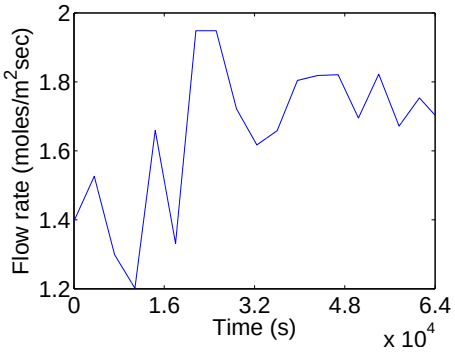

Figure 9: Flow rate (G) of the injected air provided by the LP compressor/s with time

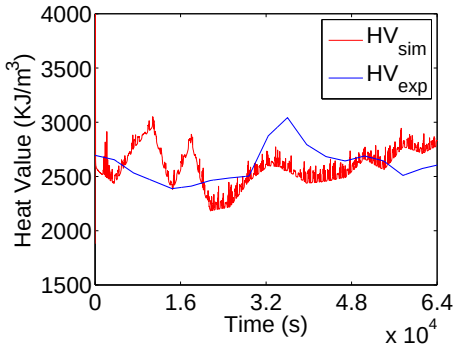

Figure 10: Experimental and simulated heating values of product gas mixture with time

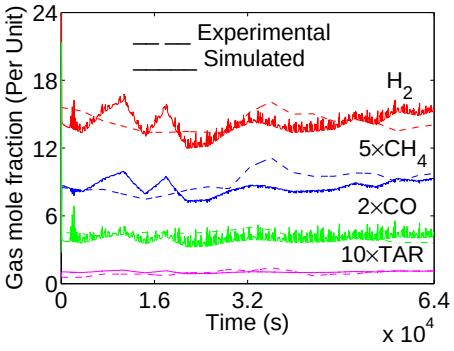

Figure 11: Experimental and simulated gas mole fraction of important gases with time

Fig. 9 shows the flow rate of inlet air supplied to the injection well. The experimental and simulated heating values of the exit gas mixture are shown in Fig. 10. A difference can be observed between simulated and experimental results. The difference can be reduced by increasing the optimization variables, which is in progress. The oscillations

in simulated results in Fig. 10 and Fig. 11 are due to the sudden increase in the solid temperature (can be seen in Fig. 3) at the reaction front for every time step. The absence of oscillations in experimental results is the result of slow sampling (data taken after every one hour). Fig. 11 shows the mole fraction of gases which contribute to the heating value.

6. Conclusion

The control oriented model of UCG is successfully developed. The solution of the model shows that the heating value of the exit gas is sensitive to flow rate of inlet gases. Therefore a robust control strategy can be employed to maintain a desired heating value in the presence of disturbances and model uncertainties by manipulating the flow rate. The solution of the model is also sensitive to the composition of inlet gas mixture, amount of steam residing in the UCG reactor and properties of coal seam. The solved model is capable of providing estimates for some important parameters of the process, which are useful for analyzing the process dynamics and in the conduction of actual field trials. The expected life of UCG reactor can also be determined by the information of the reaction front location. The input stoichiometric coefficients for coal pyrolysis reaction are optimized and results are compared with actual field trials. Despite the assumptions considered in the model the simulated results show a good match with experimental results.

Appendix A. Physical and Chemical Models

Appendix A.1. Inter Phase Transport Coefficients

The inter-phase heat transfer coefficient h determines how quickly the heat transfers from one phase to another by the process of convection. The heat transfer coefficient can be determined by following relationship [20].

$$h_T = 3C_g u_g^{0.49} T^{1.5} \left[\frac{6(1-\phi)}{d}\right]^{0.51} \times 10^{-5} \tag{A.1}$$

where d is particle diameter (m).

The inter-phase mass transfer coefficient used in the reaction rates is given by [20].

$$k_y = 0.1 h_T \tag{A.2}$$

Appendix A.2. Thermal Conductivity

The relation for effective thermal conductivity takes into account conduction in solid, radiant transfer and conduction through fluid adjacent to solid [20].

$$\begin{aligned} k &= \frac{1-\phi}{\left(\frac{1}{\lambda_s}\right) + \left(\frac{1}{25\lambda_g + dL_s}\right)} + \phi d L_v \\ L_s &= 3.16 \times 10^{-12} {T_s}^3 \\ L_v &= \frac{5.4 \times 10^{-12} {T_s}^3}{1 - 0.125\left(\frac{\phi}{1-\phi}\right)} \end{aligned} \tag{A.3}$$

where λ_s is the thermal conductivity of char (J/s/K/m), and λ_g is the thermal conductivity of H_2 (J/s/K/m).

Table A.2: Chemical reactions considered in the model

Sr	Chemical equations
1.	**Pyrolysis** $CH_aO_b \rightarrow a_{s_{2,1}} CH_{\bar{a}}O_{\bar{b}} + a_{1,1}CO + a_{2,1}CO_2 + a_{3,1}H_2 + a_{4,1}H_2O + a_{5,1}CH_4 + a_{8,1}C_9H_c$
2.	**Char Oxidation** $CH_{\bar{a}}O_{\bar{b}} + a_{7,2}O_2 \rightarrow a_{2,2}CO_2 + [a_{4,2}H_2O]$
3.	**Steam gasification** $CH_{\bar{a}}O_{\bar{b}} + a_{4,3}H_2O \rightleftharpoons a_{1,3}CO + a_{3,3}H_2$
4.	**CO_2 gasification** $CH_{\bar{a}}O_{\bar{b}} + a_{2,4}CO_2 \rightleftharpoons a_{1,4}CO + [a_{4,4}H_2O]$
5.	**Methanation** $CH_{\bar{a}}O_{\bar{b}} + a_{3,5}H_2 \rightleftharpoons [a_{1,5}CO] + a_{5,5}CH_4$
6.	**Water gas shift reaction** $a_{1,6}CO + a_{4,6}H_2O \rightleftharpoons a_{2,6}CO_2 + a_{3,6}H_2$
7.	**Oxidation of H_2** $a_{3,7}H_2 + a_{7,7}O_2 \rightarrow a_{2,7}CO_2 + a_{4,7}H_2O$
8.	**Oxidation of CO** $a_{1,8}CO + a_{7,8}O_2 \rightarrow a_{2,8}CO_2$
9.	**Oxidation of CH_4** $a_{5,9}CH_4 + a_{7,9}O_2 \rightarrow a_{2,9}CO_2 + a_{4,9}H_2O$

Appendix A.3. Chemical Model

A lot of chemical reactions take place in the UCG channel, only the set of nine important reactions is considered for describing the chemical kinetics of the model [20].

CH_aO_b and $CH_{\bar{a}}O_{\bar{b}}$ in coal pyrolysis reaction are molecular formulas for coal and char respectively. The values of a, b, $\bar{a}$, and $\bar{b}$ are determined by coal and char ultimate analysis. Reactions 2-5 are heterogeneous (char-gas) reactions where as Reactions 6-9 are homogeneous (gas-gas) reactions. The expressions for the chemical reaction rates [20] are given in the subsequent text.

Appendix A.3.1. Coal pyrolysis Reaction Rate

$$R_1 = 5\frac{\rho_1}{M_1}\exp\left(\frac{-6039}{T_s}\right) \tag{A.4}$$

where ρ_1 and M_1 are density and molecular weight of coal respectively.

Appendix A.3.2. Char Oxidation reaction Rate

$$\begin{aligned} R_2 &= \frac{1}{\frac{1}{R_{c_2}} + \frac{1}{k_y y_7}} \\ R_{c_2} &= \frac{9.55\times 10^8 \rho_2 y_7 P \exp\left(\frac{-22142}{\tilde{T}}\right)\tilde{T}^{-0.5}}{M_2} \\ \tilde{T} &= \beta T_s + (1-\beta)\,T \end{aligned} \tag{A.5}$$

where ρ_2 is char density, M_2 is the molecular weight of char and y_7 is the mole fraction of O_2. For simulations $\beta = 1$

Appendix A.3.3. Steam Gasification Reaction Rate

$$
\begin{aligned}
R_3 &= \begin{cases} \frac{1}{\frac{1}{R_{c_3}}+\frac{1}{k_y y_4}}, & \text{if } y_4 - \left(\frac{y_1 y_3}{K_{E_3}}\right) > 0 \\ \frac{1}{\frac{1}{R_{c_3}}-\frac{1}{k_y y_1}}, & \text{if } y_4 - \left(\frac{y_1 y_3}{K_{E_3}}\right) < 0 \end{cases} \\
R_{c_3} &= \frac{{R_{c_3}}^+}{y_4}\left(y_4 - \frac{y_1 y_3}{K_{E_3}}\right) \\
{R_{c_3}}^+ &= \frac{\rho_2 y_4^2 P^2 \exp\left(5.052 - \frac{12908}{\tilde{T}}\right)}{M_2\left[y_4 P + \exp\left(-22.216 + \frac{24880}{\tilde{T}}\right)\right]^2}
\end{aligned}
\tag{A.6}
$$

where y_1,y_3 and y_4 are molar fractions of CO, H_2 and H_2O respectively, and K_{E_3} is equilibrium constant for steam gasification reaction.

Appendix A.3.4. CO_2 Gasification Reaction Rate

$$
\begin{aligned}
R_4 &= \begin{cases} \frac{1}{\frac{1}{R_{c_4}}+\frac{1}{k_y y_2}}, & \text{if } y_2 - \left(\frac{y_1^2}{K_{E_4}}\right) < 0 \\ \frac{1}{\frac{1}{R_{c_4}}-\frac{2}{k_y y_1}}, & \text{if } y_2 - \left(\frac{y_1^2}{K_{E_4}}\right) > 0 \end{cases} \\
R_{c_4} &= \frac{{R_{c_4}}^+}{y_2}\left(y_2 - \frac{y_1^2}{K_{E_4}}\right) \\
{R_{c_4}}^+ &= \frac{1.15\times 10^4 \rho_2 y_2 P \exp\left(\frac{-23956}{\tilde{T}}\right)}{M_2 D} \\
D &= 1 + 0.014 y_1 P \exp\left(\frac{7549}{\tilde{T}}\right) \\
&+ \quad 0.21 y_2 P \exp\left(\frac{3171}{\tilde{T}}\right)
\end{aligned}
\tag{A.7}
$$

where y_2 is the mole fraction of CO_2, and K_{E_4} is equilibrium constant for CO_2 gasification reaction.

Appendix A.3.5. Methanation Reaction Rate

$$
\begin{aligned}
R_5 &= \begin{cases} \frac{1}{\frac{1}{R_{c_5}}+\frac{2}{k_y y_3}}, & \text{if } y_3^2 - \left(\frac{y_5}{K_{E_5}}\right) > 0 \\ \frac{1}{\frac{1}{R_{c_5}}-\frac{1}{k_y y_5}}, & \text{if } y_3^2 - \left(\frac{y_5}{K_{E_5}}\right) < 0 \end{cases} \\
R_{c_5} &= \frac{{R_{c_5}}^+}{y_3^2}\left(y_3^2 - \frac{y_5}{K_{E_5}}\right) \\
{R_{c_5}}^+ &= \frac{\rho_2 y_3^2 P^2 \exp\left(2.803 - \frac{13673}{\tilde{T}}\right)}{M_2\left[1 + y_3 P \exp\left(-10.452 + \frac{11698}{\tilde{T}}\right)\right]}
\end{aligned}
\tag{A.8}
$$

where y_5 is mole fraction of CH_4, and K_{E_5} is equilibrium constant for methanation reaction.

Appendix A.3.6. Water Gas Shift Reaction Rate

$$
\begin{aligned}
R_6 &= \begin{cases} \frac{1}{\frac{1}{R_{c_6}}+\frac{2}{kyy_1}}, & \text{if } C_1C_4 - \left(\frac{C_2C_3}{K_{E_6}}\right) > 0 \\ \frac{1}{\frac{1}{R_{c_6}}-\frac{1}{kyy_2}}, & \text{if } C_1C_4 - \left(\frac{C_2C_3}{K_{E_6}}\right) < 0 \end{cases} \\
R_{c_6} &= \frac{{R_{c_6}}^+}{C_1C_4}\left(C_1C_4 - \frac{C_2C_3}{K_{E_6}}\right) \\
{R_{c_6}}^+ &= 3\times 10^7 \phi C_1C_4 \exp\left(\frac{-7250}{\tilde{T}}\right)
\end{aligned}
\tag{A.9}
$$

where C_1, C_2, C_3 and C_4 are concentrations of CO, CO_2, H_2 and H_2O respectively, and K_{E_6} is equilibrium constant for water gas shift reaction.

Appendix A.3.7. Gas Phase Oxidation Reaction Rate

All the gas phase oxidation reactions are assigned zero rate [6].

In Eq. (A.6)-(A.9) first condition is for forward rate and second for the reverse rate.

Appendix B. Discrete Solid Phase Equations

Appendix B.1. Discrete Mass Balance For Solids

$$
{\rho_{i_x}}^{t+1} = M_i \sum_{j=1}^{9} a_{s_{ij}} r_j \times dt + {\rho_{i_x}}^t \tag{B.1}
$$

where dt is step size for time (s).

Appendix B.2. Discrete Energy Balance For Solids

$$
\begin{aligned}
{T_{s_x}}^{t+1} &= \frac{r}{C_s}\left[T^t_{s_{x+1}} - 2T^t_{s_x} + T^t_{s_{x-1}}\right] + T^t_{s_x} \\
&+ dt\frac{h}{C_s}\left[T^t_x - T^t_{s_x}\right] - dt\frac{H_s}{C_s} \\
r &= (1-\phi)\, k_s \frac{dt}{dx^2}
\end{aligned}
\tag{B.2}
$$

where dx is the step size for length (m).

The solution of above equation converges for: $r \leq \frac{1}{2}$ [23].

Acknowledgments

Authors would like to acknowledge National ICT R&D fund for providing financial support, UCG project Thar for providing technical support and all the members of control and signal processing (CASPR) research group, Muhammad Ali Jinnah University who contributed in this research work.

References

[1] B. Bose, Global energy scenario and impact of power electronics in 21st century, Industrial Electronics, IEEE Transactions on 60 (2013) 2638–2651.

[2] G. M. P. Perkins, Mathematical Modelling of Underground Coal Gasification, Ph.D. thesis, The University of New South Wales, 2005.

[3] GSP, Underground coal gasification at thar, 2013. URL: http://www.gsp.gov.pk/index.php?option=com_content&view=article&id=30.

[4] C. W. Draffin, Underground coal conversion program description, Technical Report DOE/ET-0100, United States department of energy, National Technical Information Service (NTIS) U.S. Department of Commerce 5285 Port Royal Road Springfield, Virginia 22161, 1979.

[5] K. R. Jillson, V. Chapalamadugu, B. E. Ydstie, Inventory and flow control of the {IGCC} process with {CO2} recycles, Journal of Process Control 19 (2009) 1470 – 1485.

[6] A. Khadse, M. Qayyumi, S. Mahajani, Reactor model for the underground coal gasification (ucg) channel, International Journal of Chemical Reactor Engineering 4 (2006) – ST – Reactor model for the underground coal gas.

[7] C. Magnani, S. Farouq Ali, Mathematical-modeling of stream method of underground coal gasification, Society of Petroleum Engineers Journal 15 (1975) 425 – 436.

[8] C. Magnani, S. Farouq Ali, A two-dimensional mathematical model of the underground coal gasification process, in: Fall Meeting of the Society of Petroleum Engineers of AIME, 1975.

[9] D. A. Bell, B. F. Towler, M. Fan, Chapter 5 - underground coal gasification, in: Coal Gasification and Its Applications, William Andrew Publishing, Boston, 2011, pp. 101 – 111.

[10] R. D. Gunn, D. L. Whitman, An in situ coal gasification model (forward mode) for feseability studies and design, Report of investigations, Laramie Energy Research Center, Laramie, Wyoming, 1976.

[11] A. M. Winslow, Numerical model of coal gasification in a packed bed, in: 16th Symposium on Combustion (International), 1977, pp. 503–513.

[12] C. B. Thorsness, R. B. Rozsa, Insitu coal-gasification - model calculations and laboratory experiments, Society of Petroleum Engineers Journal 18 (1978) 105–116 ST – Insitu Coal–Gasification – Model Cal.

[13] G. Perkins, V. Sahajwalla, A mathematical model for the chemical reaction of a semi-infinite block of coal in underground coal gasification, Energy & Fuels 19 (2005) 1679–1692.

[14] G. Perkins, V. Sahajwalla, Steady-state model for estimating gas production from underground coal gasification, Energy & Fuels 22 (2008) 3902–3914.

[15] E. N. J. Beizen, Modeling Underground Coal Gasification, Ph.D. thesis, Delft University of Technology, Delft, Neitherlands, 1996.

[16] K. Kostur, J. Kacur, Development of control and monitoring system of ucg by promotic, in: Carpathian Control Conference (ICCC), 2011 12th International, 2011, pp. 215 –219.

[17] K. Kostur, M. Blistanova, The research of underground coal gasification in laboratory conditions, Petroleum and Coal 51 (2009) 1–7.

[18] A. Arshad, A. Bhatti, R. Samar, Q. Ahmed, E. Aamir, Model development of ucg and calorific value maintenance via sliding mode control, in: Emerging Technologies (ICET), 2012 International Conference on, 2012, pp. 1–6.

[19] G. Herrmann, S. K. Spurgeon, C. Edwards, A model-based sliding mode control methodology applied to the hda-plant, Journal of Process Control 13 (2003) 129 – 138.

[20] C. Thorsness, E. Grens, A. Sherwood, L. L. Laboratory, A One-dimensional Model for in Situ Coal Gasification, Publication UCRL-52523, Department of Energy, Lawrence Livermore Laboratory, 1978.

[21] G. F. Froment, K. B. Bischoff, Chemical reactor analysis and design, Wiley New York, 1979.

[22] M. Hosea, L. Shampine, Analysis and implementation of tr-bdf2, Applied Numerical Mathematics 20 (1996) 21 – 37. Method of Lines for Time-Dependent Problems.

[23] W. Y. Yang, W. Cao, T.-S. Chung, J. Morris, Applied numerical methods using matlab, America 47 (2005) 509.

[24] D. Olness, L. L. N. Laboratory, The Podmoskovnaya Underground Coal Gasification Station, Lawrence Livermore Laboratory, University of California, 1981.

[25] Blinderman, M.S., Saulov, D.N., Klimenko, A.Y., Exergy optimisation of reverse combustion linking in underground coal gasification, Journal of the Energy Institute 81 (2008) 7–13.

[26] G. E. I. T. EUROPE, GAS 3100 R Coal gas/Syngas 19-3U Analyser, Gas Engineering and Instrumentation Technologies Europe, B-3380 Bunsbeek, Belgium, 2011.

[27] C. Lawrence, A. Tits, A computationally efficient feasible sequential quadratic programming algorithm, SIAM Journal on Optimization 11 (2001) 1092–1118.